The Photocatalytic Activity of the Bi_2O_3-B_2O_3-ZnO-TiO_2 Glass Coating

Do Trung Kien KIEU [1, 2], Ngoc Minh HUYNH [1, 2], Vu Uyen Nhi NGUYEN [1, 2], Quang Minh DO [1, 2*]

[1] *Department of Silicate Materials, Faculty of Materials Technology, Ho Chi Minh City University of Technology (HCMUT), 268 Ly Thuong Kiet Street, District 10, Ho Chi Minh City, VietNam*
[2] *Vietnam National University Ho Chi Minh City, Linh Trung Ward, Thu Duc City, Ho Chi Minh City, Vietnam*

http://doi.org/10.5755/j02.ms.34733

Received 28 July 2023; accepted 22 September 2023

Due to the low melting temperature, the glazes based on the Bi_2O_3-B_2O_3-ZnO system are used as coatings on the surface of industrial glass substrates. Moreover, the composition of these coatings does not contain PbO, meeting the optical and environmental properties requirements. In this study, TiO_2 was used in the Bi_2O_3-B_2O_3-ZnO glaze system to improve its photocatalytic ability. This can be considered a four – component glass system Bi_2O_3-B_2O_3-ZnO-TiO_2. The heating microscopy results show that the melting temperature of the glaze system is 606 °C. The Fourier transform infrared spectroscopy results show that the TiO_2 polyhedra are located independently in the structure without participating in forming a glass network. Thanks to that, the photocatalytic properties of TiO_2 are maintained. The X-ray diffraction patterns show that the formed TiO_2 nanocrystals are rutile and anatase crystals. The results of determining the band gap energy using UV-Vis show that the band gap energy of the base glaze system increases with the addition of TiO_2. The methylene blue decomposition results also showed that the ability to decompose organic increased when TiO_2 was added to the glaze coating. The characteristics such as melting temperature, microstructure, and photocatalytic capacity of Bi_2O_3-B_2O_3-ZnO-TiO_2 white glazes (5 and 10 % weight of TiO_2) also were indicated in this paper.
Keywords: glass coating, Bi_2O_3-B_2O_3-ZnO-TiO_2, band gap, low melting temperature, photocatalytic ability, heating microscope.

1. INTRODUCTION

The glaze is glass with low melting temperatures to coat the ceramic and glass surfaces. When designing glaze on glass surfaces, the following properties should be required: First, the softening temperature of the base glass must be low; second, for environmental protection, the glaze component does not contain toxic heavy metals such as PbO. The glazes based on the Bi_2O_3-B_2O_3-ZnO system can satisfy both requirements.

In the glass structure network of the Bi_2O_3-B_2O_3-ZnO glass system, B_2O_3 is the glass network former. Bi_2O_3, ZnO, and TiO_2 are network deformers or modified oxides. The structured boron oxide (B_2O_3) glass network is a planar consisting of complex cyclic functional groups of boroxolo, triborate, pentaborate, or tetraborate. In the boroxolo group, the coordination number of the B^{3+} ion with oxygen is 3. With the triborate, pentaborate, or tetraborate functional group, the coordination number of the B^{3+} ion is simultaneously 3 and 4. The properties of B_2O_3 glass are very complex because the formation of these functional groups is not uniform, even in the single glass composition. The structural network of the B_2O_3 glass is even more complicated when it contains modified ions in the composition. The basic structural unit of the B_2O_3 glass is the boroxole groups connected via oxygen ions. Modified ions cause the glass lattice to be broken, re-associated with different functional groups, and change the coordination number of B^{3+}. However, it can not determine the number of ions changed coordination number. Part of the $[BO_3]^{3-}$ group can be converted to $[BO_4]^{5-}$ (or B^{3+} converts from coordination number 3 to coordination 4), forming a ring of borate glass consisting of groups of three, four, or five B^{3+} ions. It is called triborate, tetraborate, pentaborate [1].

Bi_2O_3 is a modified oxide. The role of Bi_2O_3 in glass networks is complex and unclear because the $[BiO_n]^{(2n-3)-}$ polyhedra are distorted by the lone electron pairs [2]. The Bi^{3+} ions can be partially substituted for B^{3+} in the glass networks as triangles $[BiO_3]^{3-}$ and octahedral units $[BiO_6]^{9-}$. The glass networks do not form by using only Bi_2O_3 oxide, but if Bi_2O_3 and B_2O_3 oxides are melted simultaneously in one glass sample, a part of the B^{3+} ions are replaced by Bi^{3+}, creating the glass structure networks. The Bi_2O_3 glass has five fundamental oscillation positions at approximately 830, 715, 620, 450, and 350 cm^{-1} in the FTIR spectrum [3 – 5]. Bi_2O_3 has gained attention recently due to its ability to replace PbO in glass products. It is widely used in glass ceramics, thermal sensors, mechanical sensors, reflective windows, etc. [3, 5, 6]. The ZnO is also a modified oxide that reduces the melting temperature of the Bi_2O_3-B_2O_3-ZnO glass.

Bismuth (Bi) and Bi_2O_3 are also chemical compounds commonly used in photocatalytic applications. A. P. Reverberi et al. investigated the photocatalytic application of Bi_2O_3. The results show that this semiconductor can reduce environmental pollution [7]. W. Raza et al. synthesized Bi_2O_3 nanoparticles using the sol-gel method. The presence of nano Bi_2O_3 shows that the

* Corresponding author. Tel.: +848-8-661320; fax: +848-8-661843.
E-mail: *mnh_doquang@hcmut.edu.vn* (Q.M. Do)

absorption spectrum is shifted towards long wavelengths, which is very beneficial for absorbing visible light [8]. L. Zhang et al. also investigated the photocatalytic ability of Bi. At the same time, the research team also proposed methods to improve the photocatalytic ability of Bi [9]. Nano Bi also shows its photocatalytic ability and is promising for creating antibacterial materials [10]. The above studies show that Bi_2O_3 and Bi can also act as materials to enhance photocatalytic ability when combined with other traditional materials.

Furthermore, other additives added to the Bi_2O_3-B_2O_3-ZnO base frit can enhance optical properties [11, 12] and radiation shielding properties [13, 14]. Glass based on the Bi_2O_3-B_2O_3-ZnO system has a low melting temperature [15, 16], suitable for coating on various industrial glass surfaces. The Bi_2O_3-B_2O_3-ZnO glaze can be colored by mixing with the necessary pigments. For example, the white glaze is made by mixing the Bi_2O_3-B_2O_3-ZnO based frit with the TiO_2 pigment. The TiO_2 oxide is not only a colorant but also increases the chemical stability of the glaze [15, 17]. With the addition of TiO_2, the glaze has nonlinear optical properties [6, 17]. It can be used as a photocatalyst for the degradation of environmental cleaning pollutants [18 – 20].

In this study, the white glazes from the frit and TiO_2 powder (5 and 10 %) were fabricated. The melting point of the basic frit was determined by heating microscopy (HM). The microstructure was investigated by using X-ray diffraction (XRD) and Fourier transform infrared spectroscopy (FTIR) methods. The experimental data on deleting methylene blue (MB) showed the glaze's photocatalysis ability with adding TiO_2.

2. EXPERIMENTAL METHOD

The chemical compositions of the basic glaze were selected by examining the equilibrium phase diagram of the ternary system of Bi_2O_3-B_2O_3-ZnO with estimated melting temperatures according to the phase diagram in the range 590 – 600 °C [3]. The selected compositions were (wt.%): 73.79 % Bi_2O_3, 15.24 % B_2O_3, and 10.97 % ZnO. The frit fabricated from these chemical compositions is called the basic glaze and is denoted by T_0. The basic glaze was added to TiO_2 powder to fabricate a white glaze. In this study, the added TiO_2 components were 5 and 10 % weight. These white glazes were denoted as T_5 and T_{10}. The mixing ratios are shown in Table 1.

Table 1. The chemical compositions calculated from the raw mixtures

Sample	Weight percent (wt.%)			
	Bi_2O_3	B_2O_3	ZnO	TiO_2
T_0	73.79	15.24	10.97	0
T_5	70.28	14.51	10.45	4.76
T_{10}	67.08	13.85	9.97	9.10

Each batch of mixtures for T_0, T_5, and T_{10} glazes was thoroughly mixed and melted at 1200 °C for 90 min in a Pt crucible (Fig. 1 a) placed in an L5/13/P330 Nabertherm type furnace (Fig. 1 b). It is then quenched in cold water to form a new frit (Fig. 1 c). The frit was ground in a planetary mill for 120 min to obtain a fine glass powder with sizes passed through a sieve with 125 µm (Fig. 1 d). Fig. 1 shows a schema of this process.

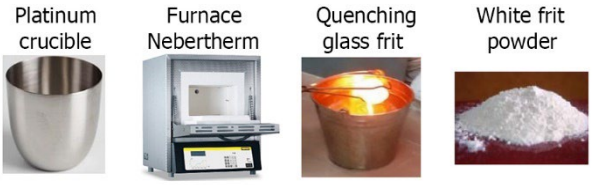

Fig. 1. The melting and quenching processes of glass frit

The melting thermal behavior of the basic frit (T_0) was studied by a Leitz HM with the standard of DIN 51730 (1998-4)/ISO 540 (1995-03-15). The device used was a Hess Instrument Corporation HM (model EM301). The test temperatures were 20 – 1200 °C with a heating velocity was 10 °C/min in the air atmosphere.

The microstructure characteristics of frits were analyzed by using XRD and FTIR. The instrument used for the XRD analysis was Bruker's D2 Phaser, the scanning 2θ angle was 20 – 80°, the scanning step was 0.02°, and the X-ray beam was CuK_α ray. The instrument used for the FTIR analysis was the Nicolet 6700 from Thermo Scientific. The scanning wavenumber was 500 – 4000 cm^{-1}, the scanning step was 0.96 cm^{-1}, and the used binder was KBr.

The absorbance of the frit samples was determined by the UV-Vis method. The UV-Vis analyzer instrument is a Lambda 950 from Perkin Elmer. The absorption spectra analysis by UV-Vis were the wavelength from 250 – 880 nm and a scanning step of 5 nm. The absorbance spectra were also used to determine the band gap energy of the frit samples. The method of determining band gap energy from the absorption spectra was mentioned by Brian D. Viezbicke et al. [21]. Accordingly, the graph showing the relationship between absorption coefficient and band gap energy is shown in Eq. 1:

$$(\alpha h\upsilon)^n = A(h\upsilon - E_g) = f(E), \quad (1)$$

where α is the molar absorptivity; h is the Planck's constant; A is the constant; υ is the frequency of light; c is the speed of light; λ is the wavelength of light; E_g is the band gap energy. The value of n was chosen to be 1/2 for the Bi_2O_3-B_2O_3-ZnO.

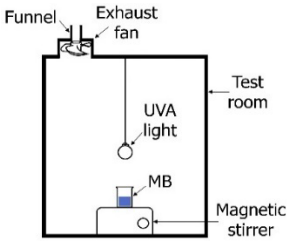

Fig. 2. Schematic diagram of the photocatalyst experiment

The photocatalytic activity of the frit powders was detected in the decomposition reaction of Methylene Blue (MB) under UV irradiation [17]. The MB was chosen because it is a common stable organic dye. Thus, if any photocatalyst decomposes MB, that photocatalyst will be able to decompose other organic substances. This experiment used the frit powder with sizes passing through a 125 µm sieve. Place two beakers containing 5 mg of frit/l MB solution (96 %) in an airtight container. Turn on the

50 W UV lamp (REPTIZOO) at different times. During illumination, beakers were magnetically stirred with a magnetic stirrer (IKA C-MAG HS) at 250 rpm. The experimental setup is shown in Fig. 2. Then, centrifuge the MB solution and compare the MB concentration in the two beakers to know the photocatalytic ability of the frit powders.

3. RESULTS AND DISCUSSION

3.1. The melting temperature of the glaze

HM images identifying shape changes with temperature are shown in Fig. 3. The basic frit (T0) softening temperature range was 487 – 552 °C, as indicated in Table 2. The melting temperature of the frit is 606 °C. It is suitable for low melting glaze coating on the glass surface. When coated at these temperature ranges, a glass product would not deform. The glaze would adhere well to the coated glass surface.

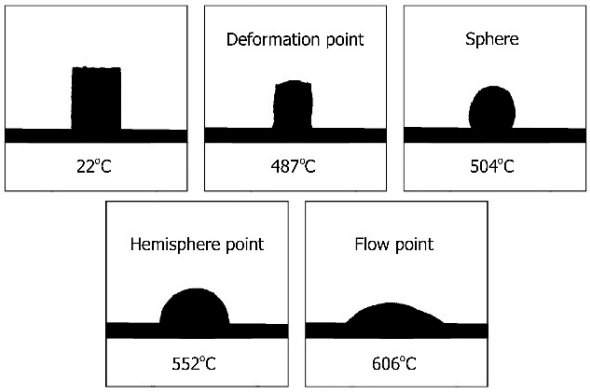

Fig. 3. The images from the heating microscopy

The temperatures obtained in Fig. 3 include: The sintering temperature was 327 °C; the softening temperature was 487 °C; the sphere temperature was 504 °C; the haft sphere temperature was 552 °C; the flow temperature was 606 °C. The melting point of frit is low and can be used as a colored glaze to coat glass surfaces.

3.2. The functional group composition of glaze

In the FTIR spectra in Fig. 4 of T_0, T_5, and T_{10}, there were the characteristic bands for symmetric stretching vibration of the Bi-O band in $[BiO_3]^{3-}$ at 715 cm^{-1} [22]. That also was the stretching vibration of the B-O band in $[BO_3]^{3-}$ group [5]. The vibrations of the bond characteristics between $[BO_4]^{5-}$ and $[BO_3]^{3-}$ groups were indicated at 880 cm^{-1} [22]. The asymmetric stretching vibration of the B–O bond in the $[BO_3]^{3-}$ group was 1146 cm^{-1} [5, 23]. The intense peak at 690.52 cm^{-1} was assigned to the Ti–O stretching band, which was the characteristic peak of TiO_2 [24]. The characteristic peaks for the bond in TiO_2 were very weak at 1377 and 1456 cm^{-1} [25]. The 1648 and 3437 cm^{-1} bands can be attributed to water content and some OH-groups. It may be due mainly to the KBr disk technique since KBr can easily absorb moisture from environmental air [23]. The corresponding peaks between T_0, T_5, and T_{10} samples were slightly shifted compared to the references. The peaks for the bond in TiO_2 were not detected on the FTIR spectra of T_0.

Thus, the structural network of the glass samples was formed from the coordination polyhedra of $[BiO_3]^{3-}$, $[BO_3]^{3-}$, and $[BO_4]^{5-}$. The $[BiO_3]^{3-}$, $[BO_3]^{3-}$, and $[BO_4]^{5-}$ groups are responsible for the Bi_2O_3-B_2O_3-ZnO glass system melting at low temperature (606 °C), as shown in Fig. 3. Y. Liu et al. have shown that the photocatalytic properties of TiO_2 may be reduced or lost if it is bonded with another element [26]. In the FITR spectrum in Fig. 4, the Ti-O bonds show that TiO_2 oxide did not form a glass network. TiO_2 exists independently in the structure so that its photocatalytic properties are maintained. This increases the photocatalytic properties of the glass coating.

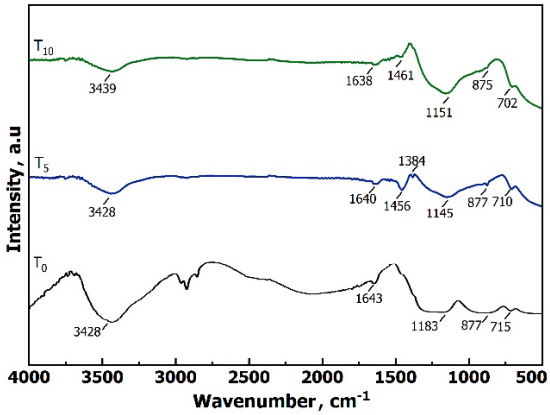

Fig. 4. FTIR spectrum of T0, T5, and T10 samples

3.3. The polymorph of TiO_2

The XRD patterns (Fig. 5) indicate that the structures of T_0, T_5, and T_{10} samples are amorphous. T5 and T10 samples also had peaks corresponding to rutile and anatase crystals. The characteristics for anatase shown in Fig. 5 were 25.22°, 38.43°, 47.85°, 53.72°, and 62.63° [27]. For rutile crystals, the characteristics were 27.34°, 36.20°, and 54.86° [28].

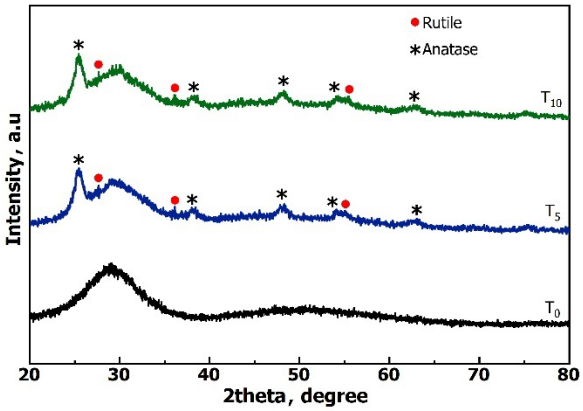

Fig. 5. XRD patterns of T0, T5, and T10 samples

Thus, TiO_2 oxide was not entirely vitrified and still exists as the anatase and rutile crystals. Estimating the crystal sizes using the Sherrer formula [29] showed that the crystal size of anatase was 9.58 – 10.21 nm and rutile was 13.76 – 22.09 nm. In other words, in the T_5 and T_{10} samples, the anatase and rutile nanocrystals dispersed in the amorphous field of the Bi_2O_3-B_2O_3-ZnO basic glass system. The anatase and rutile nanocrystals influence the photocatalytic applicability of this glass system.

3.4. Ability to absorb light and the band gap energy

Fig. 6 is the UV-vis absorption spectrum of the frit samples. Compared with T_0 sample, T_5 and T_{10} samples were changed very complexly regarding absorption capacity. Absorption capacity can be divided into three regions: (1) ultraviolet, (2) Visibility from 380 – 550 nm, and (3) visible from 550 – 780 nm.

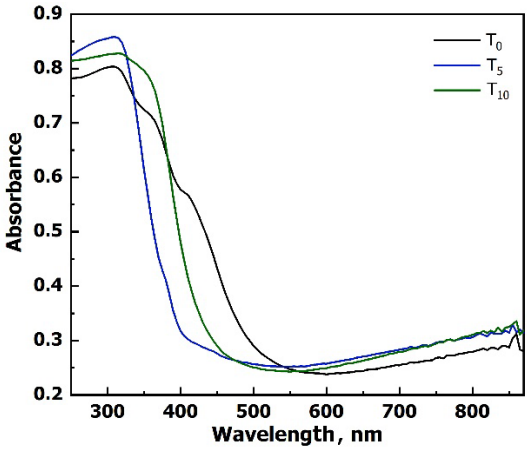

Fig. 6. Absorbance spectrum of T0, T5, and T10 samples

The presence of Ti^{3+} ions and the Ti^{3+}/Ti^{4+} ratio affect the absorbance, but they were not determined in these experiments. In literature, Duffy [30] showed that the influence of TiO_2 on optical properties was dominated by the molar electronic polarization of the Ti^{4+} ions. Usually, the Ti^{4+} ion had greater electron polarization than other components of the base glass [31]. Absorbance was in the visible region from 380 to 780 nm. It varied according to TiO_2 content, and the ratio of the Ti^{3+}/Ti^{4+} ions. Glass that does not contain the Ti^{3+} ions would produce a blue to violet color [32]. The charge of the Ti^{4+} ions increases with increasing TiO_2 content [32 – 34], giving the glass a yellow color.

Thus, the TiO_2 oxide dramatically affects the optical properties of the basic frit system. The gap band energies (E_g) of T_0, T_5, and T_{10} samples were calculated to clarify this effect. The second derivative equation of the function *f(E)* (1) has been established (Eq. 2). The root of this equation is the coordinates of the inflection point of the function *f(E)*. The intersection of the tangent of the function *f(E)* at the inflection point and the horizontal axis is the value E_g. The calculated results of E_g from the absorption spectrum in Fig. 7 show that the band gaps of T_0, T_5, and T_{10} samples are 2.098, 2.478, and 2.695 eV, respectively.

$$f''(E) = 0. \quad (2)$$

In some previous studies [17], TiO_2 reduced the band gap energy of the basic glass. The low E_g in the literature could be explained by a large amount of network modifier species variations in the coordination environment of TiO_2 oxide [12]. The reason was that TiO_2, as a modified oxide, creates structural errors. As a result, the conduction and valence band gap has been narrowed. The expression of TiO_2 involved in glass structure formation as TiO_2 crystals was not detected on XRD patterns. In this study, anatase and rutile nanocrystals were distributed in the amorphous field of the Bi_2O_3-B_2O_3-ZnO glass, as shown in the XRD samples.

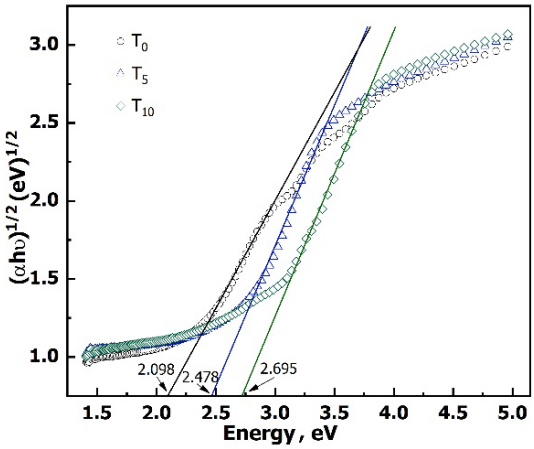

Fig. 7. The band gap energies of T0, T5, and T10 samples

The bandgap energy has increased compared to the base glass. That was 2.478 eV for 5 % TiO_2 and 2.695 eV for 10 % TiO_2 compared to 2.098 eV for 0 % TiO_2. In the literature, this phenomenon can be explained by the nanoparticle size or the tunneling effect [35 – 37].

3.5. Ability to decompose methylene blue

The E_g values of T_0, T_5, and T_{10} glass samples indicated their photocatalytic ability. MB decomposition experiment with these glasses was performed to demonstrate the photocatalytic ability. Fig. 8 shows the results of the MB decomposition at different times.

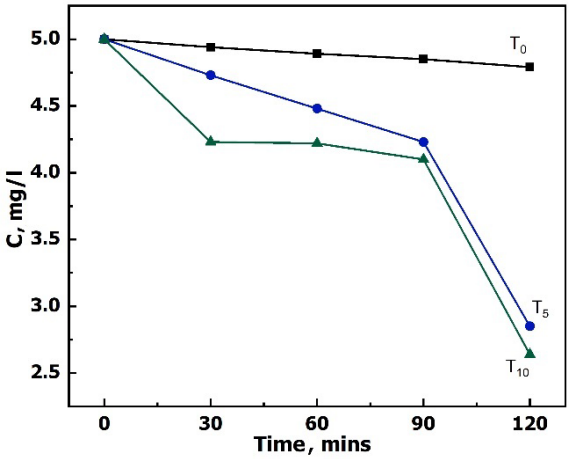

Fig. 8. The decomposed MB concentrations under the UV irradiation over time

The MB decomposition of the T_0 sample was very poor, although its E_g is smaller than that of the T_5 and T_{10} samples. The best MB decomposition was that of T_{10} sample, although its E_g was higher than that of the T_5 and the T_0 samples. It could be explained by the photocatalytic reaction and the ability to excite the electron to the conduction band. It was also able to conduct this electron to the reaction region. In this respect, anatase and rutile nanocrystals of T_5, T_{10} performed better than T_0 sample.

The decomposition of organic matter by TiO_2 can be explained as follows. When TiO_2 is excited, electrons jump from the conduction band to the valence band. Holes (h^+)

and electrons (e^-) will form. They will ionize water and oxygen in the air. The •OH and $•O_2^-$ ions will create the ability for TiO_2 to decompose organic matter. The above process can be described in Fig. 9.

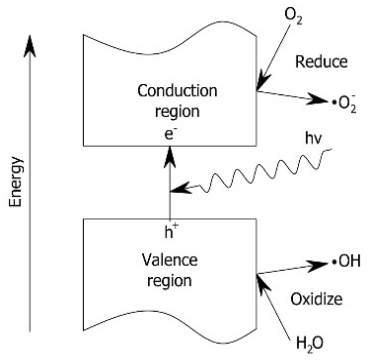

Fig. 9. Photocatalytic mechanism of TiO_2

4. CONCLUSIONS

A white glaze based on the Bi_2O_3-B_2O_3-ZnO-TiO_2 system was made by the conventional melting and quenching technique. These glazes had low melting points and could be used as a color under the glaze to coat glass surfaces. In other words, Bi_2O_3 can completely replace PbO as a colored glaze with a low melting temperature, only about 600 °C. The study of its photocatalytic characteristics was demonstrated by the MB decomposition. The experimental results show that the Bi_2O_3-B_2O_3-ZnO-TiO_2 glaze coating could be self-cleaning in the environment due to the decomposition of organic substances on the surface. Furthermore, with TiO_2 in the composition and a relatively low Eg value, approximately that of a semiconductor, the bactericidal ability of this type of glaze is entirely possible. Among the components, the TiO_2 nanocrystals played a decisive role in photocatalytic performance. In addition to its effect as a low-melting temperature glaze, the Bi_2O_3-B_2O_3-ZnO-TiO_2 glass material can be used as a photocatalyst.

Acknowledgments

We acknowledge Ho Chi Minh City University of Technology (HCMUT), VNU-HCM for supporting this study.

REFERENCES

1. **Silver, A.H., Bray, P.J.** Nuclear Magnetic Resonance Absorption in Glass. I. Nuclear Quadrupole Effects in Boron Oxide, Soda-Boric Oxide, and Borosilicate Glasses *The Journal of Chemical Physics* 29 (5) 1958: pp. 984 – 990. https://doi.org/10.1063/1.1744697
2. **Bale, S., Rahman, S., Awasthi, A., Sathe, V.** Role of Bi_2O_3 Content on Physical, Optical and Vibrational Studies in Bi_2O_3-ZnO-B_2O_3 Glasses *Journal of Alloys and Compounds* 460 (1 – 2) 2008: pp. 699 – 703. https://doi.org/10.1016/j.jallcom.2007.06.090
3. **Bale, S., Rao, N.S., Rahman, S.** Spectroscopic Studies of Bi_2O_3-Li_2O-ZnO - B_2O_3 Glasses *Solid State Sciences* 10 (3) 2008: pp. 326 – 331. https://doi.org/10.1016/j.solidstatesciences.2007.09.017
4. **He, F., He, Z., Xie, J., Li, Y.** IR and Raman Spectra Properties of Bi_2O_3-ZnO-B_2O_3-BaO Quaternary Glass System *American Journal of Analytical Chemistry* 5 (16) 2014: p. 1142. https://doi.org/10.4236/ajac.2014.516121
5. **He, F., Cheng, J.S., Deng, D.W., Wang, J.** Structure of Bi_2O_3-ZnO-B_2O_3 System Low-Melting Sealing Glass *Journal of Central South Univerity of Technology* 17 2010: pp. 257 – 262. https://doi.org/10.1007/s11771-010-0039-x
6. **Sousa, N.D., Araújo, M., Jacinto, C., Vermelho, M.V.D.** The Role of TiO_2 in the B_2O_3-Na_2O-PbO-Al_2O_3 Glass System *Journal of Solid State Chemistry* 184 (11) 2011: pp. 3062 – 3065. https://doi.org/10.1016/j.jssc.2011.09.011
7. **Reverberi, A.P., Varbanov, P.S.V., Vocciante, M., Fabiano, B.** Bismuth Oxide-Related Photocatalysts in Green Nanotechnology: A Critical Analysis *Frontiers of Chemical Science and Engineering* 12 2018: pp. 878 – 892. https://doi.org/10.1007/s11705-018-1744-5
8. **Raza, W., Haque, M.M, Muneer, M., Harada, T., Matsumura, M.** Synthesis, Characterization and Photocatalytic Performance of Visible Light Induced Bismuth Oxide Nanoparticle *Journal of Alloys and Compounds* 648 2015: pp. 641 – 650. https://doi.org/10.1016/j.jallcom.2015.06.245
9. **Zhang, L., Li, Y., Li, Q., Fan, J., Carabineiro, S.A.C., Lv, K.** Recent Advances on Bismuth-Based Photocatalysts: Strategies and Mechanisms *Chemical Engineering Journal* 419 2021: p. 129484. https://doi.org/10.1016/j.cej.2021.129484
10. **Zhao, H., Tian, F., Wang, R., Chen, R.** A Review on Bismuth-Related Nanomaterials for Photocatalysis *Reviews in Advanced Sciences and Engineering* 3 (1) 2014: pp. 3 – 27. https://doi.org/10.1166/rase.2014.1050
11. **Sumalatha, B., Omkaram, I., Rao, T.R., Raju, C.L.** Alkaline Earth Zinc Borate Glasses Doped with Cu^{2+} Ions Studied by EPR, Optical and IR Techniques *Journal of Non-Crystalline Solids* 357 (16 – 17) 2011: pp. 3143 – 3152. https://doi.org/10.1016/j.jnoncrysol.2011.05.005
12. **Saritha, D., Markandeya, Y., Salagram, M., Vithal, M., Singh, A., Bhikshamaiah, G.** Effect of Bi_2O_3 on Physical, Optical and Structural Studies of ZnO-Bi_2O_3-B_2O_3 Glasses *Journal of Non-Crystalline Solids* 357 (52 – 54) 2008: pp. 5573 – 5579. https://doi.org/10.1016/j.jnoncrysol.2008.09.017
13. **Sayyed, M., Tekin, H.O., Taki, M.M., Mhared, M.H.A., Agar, O., Sakar, E., Kaky, K.M.** Bi_2O_3-B_2O_3-ZnO-BaO-Li_2O Glass System for Gamma Ray Shielding Applications *Optik* 201 2020: p. 163525. https://doi.org/10.1016/j.ijleo.2019.163525
14. **Sangwaranatee, N., Cheewasukhanont, W., Limkitjaroenporn, P., Borisut, P., Wongdamnern, N., Khrongchaiyaphum, F., Kothan, S., Kaewkhao, J.** Development of Bismuth Alumino Borosilicate Glass for Radiation Shielding Material *Radiation Physics and Chemistry* 186 2021: p. 109542. https://doi.org/10.1016/j.radphyschem.2021.109542
15. **Fredericci, C., Yoshimura, H., Molisani, A., Fellegara, H.** Effect of TiO_2 Addition on the Chemical Durability of Bi_2O_3-SiO_2-ZnO-B_2O_3 Glass System *Journal of Non-Crystalline Solids* 354 (42 – 44) 2008: pp. 4777 – 4785. https://doi.org/10.1016/j.jnoncrysol.2008.04.026

16. **Gu, Q.B., Ni, J.M.** Preparation and Analysis of Doped TiO_2 in the Bi_2O_3-SiO_2-ZnO-B_2O_3 Low-Melting Sealing Glasses *Key Engineering Materials* 509 2012: pp. 308 – 313. https://doi.org/10.4028/www.scientific.net/KEM.509.308
17. **Kirdsiri, K., Srisittipokakun, N., Ruangtaweep, Y., Boonin, K., Limsuwan, P., Kaewkhao, J.** Effect of Addition TiO_2 on Bi_2O_3-TiO_2-B_2O_3 Glasses *Advanced Materials Research* 770 2013: pp. 72 – 75. https://doi.org/10.4028/www.scientific.net/AMR.770.72
18. **Avciata, O., Benli, Y., Gorduk, S., Koyun, O.** Ag Doped TiO_2 Nanoparticles Prepared by Hydrothermal Method and Coating of the Nanoparticles on the Ceramic Pellets for Photocatalytic Study: Surface Properties and Photoactivity *Journal of Engineering Technology and Applied Sciences* 1 (1) 2016: pp. 34 – 50. https://doi.org/10.30931/jetas.281381
19. **Amin, M.A., Dey, S.C., Rashid, T.U., Ashaduzzaman, M., Shamsuddin, S.M.** Solar Assisted Photocatalytic Degradation of Reactive Azo Dyes in Presence of Anatase Titanium Dioxide *International Journal of Latest Research in Engineering and Technology* 2 (3) 2016: pp. 14 – 21.
20. **Quang, M.D., Hong, D.T.T., Vi, N.N.T.** Antibacterial and Photocatalytic Ability of the Ag/TiO_2 Coating on the Glass Surface *Vietnam Journal of Science and Technology* 57 (3A) 2019: pp. 1 – 10. https://doi.org/10.15625/2525-2518/57/3A/13936
21. **Sallam, O., Madbouly, A., Elalaily, N., Eldin, F.E.** Physical Properties and Radiation Shielding Parameters of Bismuth Borate Glasses Doped Transition Metals *Journal of Alloys and Compounds* 843 2020: pp. 156056. https://doi.org/10.1016/j.jallcom.2020.156056
22. **Ardelean, I., Cora, S., Rusu, D.** EPR and FT-IR Spectroscopic Studies of Bi_2O_3-B_2O_3-CuO Glasses *Physica B: Condensed Matter* 403 (19 – 20) 2008: pp. 3682 – 3685. https://doi.org/10.1016/j.physb.2008.06.016
23. **Gabr, M., Ali, K.A.A., Mostafa, A.G.E.D.** Infrared Analysis and Physical Properties Studies of B_2O_3-CaO-ZnO-TiO_2 Glass System *Turkish Journal of Physics* 31 (1) 2007: pp. 31 – 40. https://journals.tubitak.gov.tr/physics/vol31/iss1/4
24. **Abbad, M.M.B., Kadhum, A.A.H., Mohamad, A.B., Takriff, M.S., Sopian, K.** Synthesis and Catalytic Activity of TiO_2 Nanoparticles for Photochemical Oxidation of Concentrated Chlorophenols Under Direct Solar Radiation *International Journal of Electrochemical Science* 7 2012: pp. 4871 – 4888. https://doi.org/10.1016/S1452-3981(23)19588-5
25. **Frank, S.N., Bard, A.J.** Heterogeneous Photocatalytic Oxidation of Cyanide Ion in Aqueous Solutions at Titanium Dioxide Powder *Journal of the American Chemical Society* 99 (1) 1977: pp. 303 – 304. https://doi.org/10.1021/ja00443a081
26. **Liu, Y., Li, Y., Yang, S., Lin, Y., Zuo, J., Liang, H., Peng, F.** Revealing the Relationship between Photocatalytic Properties and Structure Characteristics of TiO_2 Reduced by Hydrogen and Carbon Monoxide Treatment *Chemistry Sustainability Energy Materials* 11 (16) 2018: pp. 2766 – 2775. https://doi.org/10.1002/cssc.201800940
27. **Hussein, F.H., Halbus, A.F.** Rapid Decolorization of Cobalamin *International Journal of Photoenergy* 2012 2012: p. 495435. https://doi.org/10.1155/2012/495435
28. **Djokic, V.R., Marinkovíc, A.D., Petrovíc, R.D., Ersen, O., Zafeiratos, S., Mitríc, M., Ophus, C., Radmilovíc, V.R., Janáckovíc, D.T.** Highly Active Rutile TiO_2 Nanocrystalline Photocatalysts *ACS Applied Materials and Interfaces* 12 (29) 2020: pp. 33058 – 33068. https://doi.org/10.1021/acsami.0c03150
29. **Kibasomba, P.M., Dhlamini, S., Maaza, M., Liu, C.P., Rashad, M.M., Rayan, D.A., Mwakikunga, B.W.** Strain and Grain Size of TiO_2 Nanoparticles from TEM, Raman Spectroscopy and XRD: The Revisiting of the Williamson-Hall Plot Method *Results in Physics* 9 2018: pp. 628 – 635. https://doi.org/10.1016/j.rinp.2018.03.008
30. **Duffy, J.A.** Refractivity and Coordination Number Changes of the Ti^{4+} Ion in Glass *Physics and Chemistry of Glasses European Journal of Glass Science and Technology Part B* 47 (5) 2006: pp. 582 – 587.
31. **Duffy, J.A.** The Electronic Polarisability of Oxygen in Glass and the Effect of Composition *Journal of Non-Crystalline Solids* 297 (2 – 3) 2002: pp. 275 – 284. https://doi.org/10.1016/S0022-3093(01)00940-1
32. **Richter, S., Moncke, D., Zimmermann, F., Kamitsos, E.I., Wondraczek, L., Tunnermann, A., Nolte, S.** Ultrashort Pulse Induced Modifications in ULE - from Nanograting Formation to Laser Darkening *Optical Materials Express* 5 (8) 2015: pp. 1834 – 1850. https://doi.org/10.1364/OME.5.001834
33. **Dejneka, M., Dutta, I., Smith, C.** Chemically Strengthened Low Crystallinity Black Glass – Ceramics with High Liquidus Viscosities *International Journal of Applied Glass Science* 5 (2) 2014: pp. 146 – 160. https://doi.org/10.1111/ijag.12076
34. **Chavoutier, M., Caurant, D., Majerus, O., Boulesteix, R., Loiseau, P., Jousseaume, C., Brunet, E., Lecomte, E.** Effect of TiO_2 Content on the Crystallization and the Color of (ZrO_2, TiO_2) - Doped Li_2O-Al_2O_3-SiO_2 Glasses *Journal of Non-Crystalline Solids* 384 2014: pp. 15 – 24. https://doi.org/10.1016/j.jnoncrysol.2013.03.034
35. **Diamantopoulos, N.C., Barnasas, A., Garoufalis, C.S., Anyfantis, D.I., Bouropoulos, N., Poulopoulos, P., Baskoutas, S.** Band Gap Measurements of Nano-Meter Sized Rutile Thin Films *Nanomaterials* 10 (12) 2020: p. 2379. https://doi.org/10.3390/nano10122379
36. **Sasaki, T., Watanabe, M.** Semiconductor Nanosheet Crystallites of Quasi-TiO_2 and Their Optical Properties *The Journal of Physical Chemistry B* 101 (49) 1997: pp. 10159 – 10161. https://doi.org/10.1021/jp9727658
37. **Sato, H., Ono, K., Sasaki, T., Yamagishi, A.** First-Principles Study of Two-Dimensional Titanium Dioxides *The Journal of Physical Chemistry B* 107 (36) 2003: pp. 9824 – 9828. https://doi.org/10.1021/jp035017t